Characterizing Limits of Vision-Based Force Feedback in Simulated Surgical Tool-Tissue Interaction

Kevin Huang, Digesh Chitrakar, Rahul Mitra, Divas Subedi, Yun-Hsuan Su

***Abstract*— Haptic feedback can render real-time force interactions with computer simulated objects. In several telerobotic applications, it is desired that a haptic simulation reflects a physical task space or interaction accurately. This is particularly true when excessive applied force can result in disastrous consequences, as with the case of robot-assisted minimally invasive surgery (RMIS) and tissue damage. Since force cannot be directly measured in RMIS, non-contact methods are desired. A promising direction of non-contact force estimation involves the primary use of vision sensors to estimate deformation. However, the required fidelity of non-contact force rendering of deformable interaction to maintain surgical operator performance is not well established. This work attempts to empirically evaluate the degree to which haptic feedback may deviate from ground truth yet result in acceptable teleoperated performance in a simulated RMIS-based palpation task. A preliminary user-study is conducted to verify the utility of the simulation platform, and the results of this work have implications in haptic feedback for RMIS and inform guidelines for vision-based tool-tissue force estimation. An adaptive thresholding method is used to collect the minimum and maximum tolerable errors in force orientation and magnitude of presented haptic feedback to maintain sufficient performance.**

***Keywords*— haptic feedback, user studies, minimally invasive surgery, bio-robotics**

I. Introduction

This work investigates the effects of disparity between rendered haptic feedback and visual feedback when interacting with deformable bodies, and is motivated by the use case of RMIS. While teleoperated architectures of robotic surgery offer benefits, the lack of force feedback is a remaining challenge [1]. In telerobotic surgery, direct sensing of haptic sensations is not a possibility - sterilization requirements would make tool-tip sensors impractical [2]. Instead, surgeons currently navigate surgical tools and estimate surgery state based on vision alone.

On the other hand, non-contact force estimation via vision sensors is a promising alternative [3]. Figure 1 depicts the workflow of non-contact, vision-based force estimation scenarios that motivate the experimental question in this work. In this paper, the degree to which indirect force acquisition may deviate from ground truth yet enable sufficient teleoperator performance is investigated.

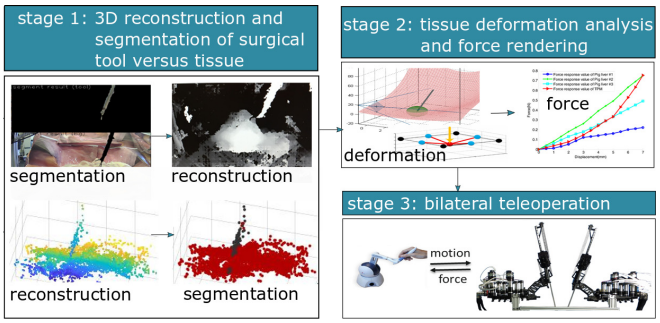

Fig. 1: The vision-based non-contact force estimation pipeline for RMIS haptic feedback that consists of three stages [4].

A. Related Work

1) Haptic User Studies: Psychophysical studies aim to ascertain the relationship between stimuli and human perception to said stimuli. They have been successfully used to extrapolate the thresholds of human haptic perception [5]. Examples include determining thresholds for the just-noticeable-difference in multi-digit haptic devices [6], the sensation of roundness in spheres [7], relocation of vibrotactile haptic feedback [8], and asynchrony between visual and haptic feedback [9] to name a few. These studies have implications in the design of haptic feedback in the application spaces of prostheses [10], user interfaces [11], [12], virtual reality and more.

In teleoperation, haptic virtual fixtures can be used to overlay intelligent force feedback on other sensory modalities. Virtual fixtures can be classified into two types, including forbidden region virtual fixtures and guidance virtual fixtures. The former is used to prevent a teleoperator from entering a delicate region, while the latter can guide a user along a desired trajectory [13]. These fixtures can be created based on real-time sensory information [14], known geometries [15], or robot kinematic state [16], for example.

2) Vision-Based Force Estimation in RMIS: There is strong research interest in determining mechanical characteristics of biological tissue for both histological and pathological considerations in medical diagnostics and MIS [17]. In laparoscopic liver surgery, for instance, internal tissue palpation serves as an essential preoperative procedure that reveals issues such as presence of emphysema with an associated depressed diaphragm, fatty infiltration, active

Kevin Huang, Digesh Chitrakar, Rahul Mitra, and Divas Subedi are with Trinity College, Dept. of Engineering, 300 Summit St, Hartford, CT 06106 USA {kevin.huang, digesh.chitrakar, rahul.mitra, divas.subedi}@trincoll.edu

Yun-Hsuan Su is with Mount Holyoke College Department of Computer Science, 50 College St, South Hadley, MA 01075 USA.

hepatitis, cirrhosis and hepatic neoplasm [18]. Furthermore, surgeon response to both visual and haptic cues inform safe practices. Since robotics were introduced to surgery, assistance functions like tremor reduction [19], [20], motion scaling [21] and haptic guidance along pre-planned surgical trajectories through virtual fixtures [22] have been tested in operating room teleoperation settings. These technologies target a broad spectrum of medical applications ranging from thoracic surgery, ophthalmic surgery, laparoscopic surgery, otorhinolaryngology, orthopedics and neurosurgery [23].

Due to the teleoperated nature of RMIS, one major drawback is the loss of direct force information from the surgical tool-tissue contact [24], [25], which provides cues for surgeons in manual surgery. Since direct force measurement is not amenable to sterilization procedures in surgery [2], researchers seek alternative approaches to estimate contact force. One promising approach is vision-based force estimation, namely, a pipeline that predicts contact force from real-time tissue deformation analysis from vision [4]. Some researchers in the field have been investigating whether a data-driven [26], [27] or a model-based approach [28] leads to greater accuracy in force estimation. Another line of research targets autonomous camera positioning to provide optimal 3D tissue surface reconstruction [29], [30].

B. Contributions

To the best of the authors' knowledge, this work is the first to

i) simulate model-based deformable object haptic interaction and systematically degrade haptic feedback;
ii) evaluate via a preliminary user study the boundaries of acceptable user performance along parameters of force feedback degradation in orientation and magnitude.

Uncertainties exist in vision-based force estimation, which could result in deviated direction or magnitude. This motivates the authors' study of error thresholds in haptic feedback for successful task execution.

II. Methods

A. Tissue Model

Several approaches to modeling human tissue exist, including deformable splines, linked volumes [31], and mass spring models [32]. Some techniques incorporate nonlinear properties [33], including the Maxwell-Weichert model [34]. In this work, the examined tissue was modeled using an adapted version of the 2 degrees of freedom (DOF) mass-spring-damper (MSD) model of the Capsule of Glisson as described by Boux de Casson et al. The original model considers viscous-elastic response to elongation and torsional interactions between nodes in a mesh [35].

The tissue for this work was also simulated as a lumped second order MSD mathematical model. In total, 100 points masses (nodes) were used to generate a 10×10 square deformable mesh representing the palpation surface. This arrangement is shown in Fig. 2.

Nodes and directly neighboring nodes were interfaced with 3DOF spring and damping elements. These included the original elongation and torsional components, as well as the addition of flexion viscous-elastic effects. All 100 nodes at rest and without disturbance lie in a single plane, and the four nodes constituting the corners of the square mesh were fixed or grounded in space. Symbolically, each node pair can be represented with translational and rotational elements as shown in Fig. 3.

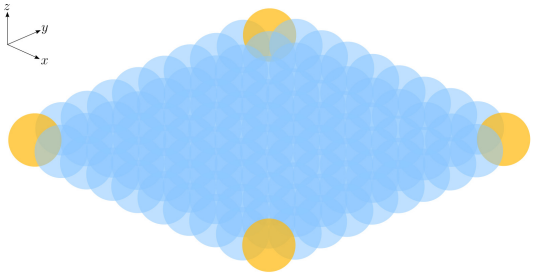

Fig. 2: Square mesh MSD model. At rest nodes all lie within a single plane and corner nodes (gold) are fixed in place.

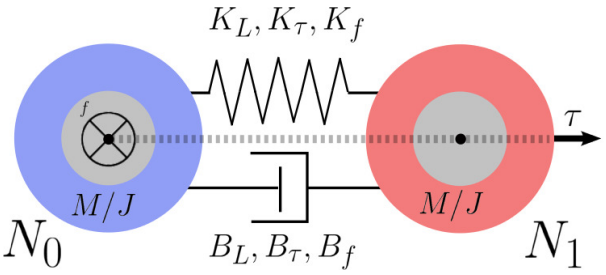

Fig. 3: Translational and rotational physical elements that govern node-to-node (N_0 and N_1 are nodes) dynamic interaction. M,J are translational and rotational inertias, and K_L,K_τ,K_f and B_L,B_τ,B_f are linear spring and damping coefficients for translation, torsion and flexion respectively.

Rotational dynamics are defined along two axes, which are displayed as f,τ in Fig. 3. f points into the page, and determines flexion dynamics, while τ is used for torsional components. All nodes have identical translational and rotational inertias, denoted M,J respectively.

Capsule of Glisson dynamics are thus described in equations (1)-(5). For each node N_i, first determine the net torque via a linear second-order viscous-elastic model, i.e.

$$\vec{\tau}_i = J(\ddot{\theta}_f + \ddot{\theta}_\tau) + K_f\theta_f + B_f\dot{\theta}_f + K_\tau\theta_\tau + B_\tau\dot{\theta}_\tau \qquad (1)$$

where θ_f, θ_τ are the vectorized relative angular position about axes f and τ respectively. The translational dynamics between two nodes, such as N_0 and N_1 shown in Fig. 3 are then determined as

$$\vec{F}_{\text{net}} = \vec{F}_L + \vec{F}_{\text{rot}} \qquad (2)$$

$$\vec{F}_L = K_L\left(\|\vec{l}_{01}\|_2 - \|\vec{l}_i\|_2\right)\hat{l} + B_L\frac{d}{dt}\|\vec{l}_{01}\|_2\hat{l} + \qquad (3)$$

$$+M\frac{d^2}{dt^2}\|\vec{l}_{01}\|_2\hat{l} \qquad (4)$$

$$\vec{F}_{\text{rot}} = \vec{\tau}_1 \times \frac{\vec{l}_{10}}{\|\vec{l}_{10}\|_2} - \vec{\tau}_0 \times \frac{\vec{l}_{01}}{\|\vec{l}_{01}\|_2} \qquad (5)$$

where $\vec{F}_L$ and $\vec{F}_{\text{rot}}$ are translational forces due to elongation and rotational components respectively and $\vec{l}_{01}$ is the vector from node N_0 to N_1 with unit vector $\hat{l}$ and initial state $\vec{l}_i$.

B. Tissue Simulation

The tissue simulation incorporated the above lumped second-order mathematical representation for tissue dynamics. 3DOF haptic rendering was achieved using the proxy method of force feedback - both proxy and user input were implemented as spheres. OpenGL was used to render a surface mesh with vascular tissue to simulate a robotic surgical scenario [36]. A surgical tool tip was graphically rendered as the user proxy object, and a green patch on the tissue surface indicated the region of interest (ROI). Excessive force or tool-penetration resulted in pop-through and failure. CHAI3D and the Sensable PHANToM Omni 3 DOF haptic device were used to render force feedback. The simulated tool-tissue interaction is shown in Fig. 4.

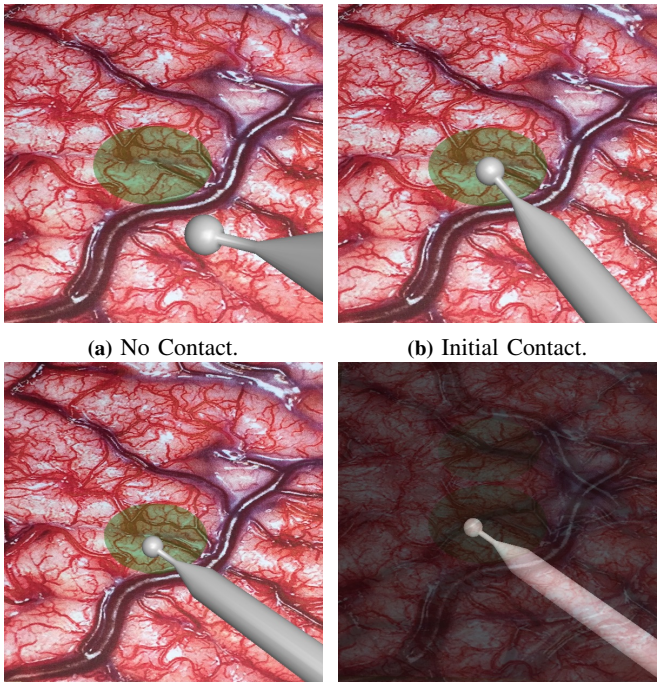

(a) No Contact. **(b)** Initial Contact. **(c)** Palpation Deformation. **(d)** Pop-through.

Fig. 4: Examples of the simulated tool-tissue interaction. The tool initiates contact and increases penetration depth into the tissue from (a) → (d) until pop-through, representing tissue-damage. The green patch indicates the ROI. Visual cues of deformation can be observed between (b) and (c). With pop-through (d), the tissue is rendered transparent to signify failure/tissue damage.

C. User Study

A preliminary user study was conducted to evaluate the fidelity requirements for non-contact force estimation. Three variations in rendered force were investigated:

i) orientation
   a. (**A**) tilted towards or away from user;
   b. (**B**) about the visual axis, CCW or CW;
ii) (**C**) magnitude.

Positive and negative thresholds for satisfactory performance along these parameters were sought in this study. The three test variations, each with two test directions, are depicted graphically in Fig. 5.

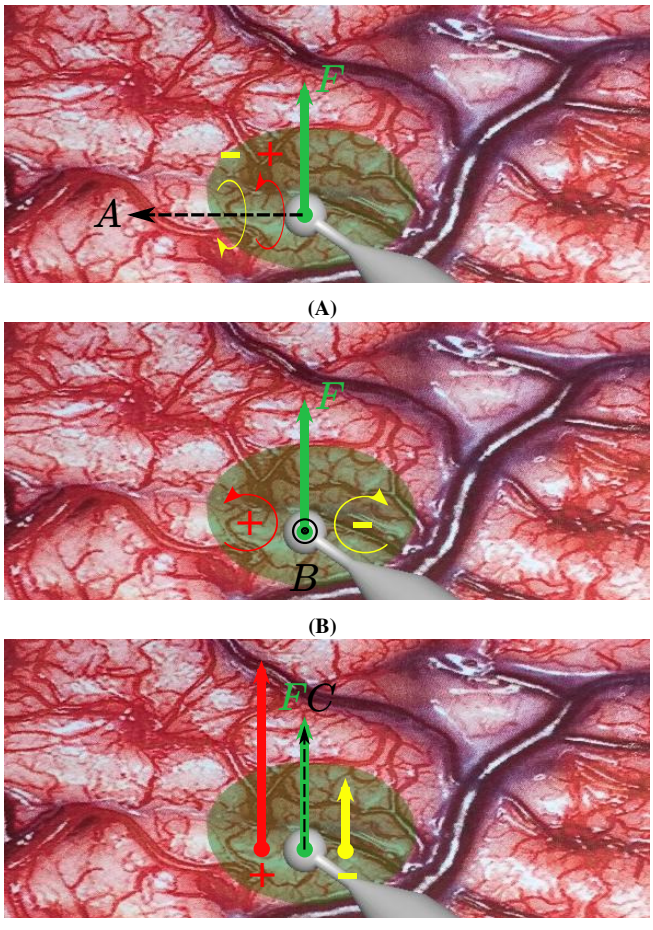

Fig. 5: Positive and negative directions for test parameters **A**, **B**, and **C**. **Green** indicates the ground truth force vector based on simulated physics, **red** and **yellow** indicate positive and negative error directions respectively. **Black** indicates axis of error parameter. For **A**, positive error tilts the force vector into the page, and negative error tilts the force out of the page. As viewed from the user, positive error in **B** rotates the force vector CCW, and negative error CW. Parameter **C** scales the magnitude of the perceived force.

1) Subject Recruitment: In this preliminary user study, a total of four members of the Trinity College community voluntarily agreed to participate. Recruitment was achieved via word of mouth and was approved by the Trinity College internal review board. Participants were all right-handed and proficient with computers and video games. No participants were actual trained surgeons.

2) Experimental Procedure, Adaptive Thresholding: To start, subjects were required to familiarize themselves with the palpation task with no degradation in haptic feedback. The goal was for users to palpate the target with maximum exerted force without damaging the tissue, i.e. pop-through. Success requires users to reach within a predefined δ threshold of the maximum allowed force, and users needed to demonstrate success in ten successive runs to proceed to the experimental task. In this work, a palpation force of 2.1 N

or greater was deemed a success (pop through occurred at 2.3N). Each condition was tested three times per trial; the user passed if he/she both succeeded in at least two out of the three runs and none of the three runs popped-through.

The experimental portion of the task implemented an adaptive thresholding method described here. Suppose a ground truth, non-altered value of $\mathscr{Y}$ for parameter $\mathbb{Y}$ (e.g. $\mathscr{Y} = 0^\circ$ for $\mathbb{Y}$ the orientation error, and $\mathscr{Y} = 1$ for $\mathbb{Y}$ the force magnitude scaling factor). The experiment begins at initial deviation $y[0]$ from $\mathscr{Y}$, i.e. the applied test condition at iteration zero is $\mathscr{Y} - y[0]$.

The subsequent test condition depends on the user's success or failure of the current condition. This sequence is formulated with adaptive thresholding in (6) as

$$y[i] = y[i-1] - y[0]\sigma(i-1)K^i \tag{6}$$

where

$$\sigma(m) = \begin{cases} -1 & \text{trial } y[m] \text{ was a success} \\ 1 & \text{trial } y[m] \text{ was a failure} \end{cases}$$

and K is the adaptive rate. In this study $K = 0.49411$. With repeated failures, a subject would return to a final experimental condition within $0.025 \cdot y[0]$ (or one fortieth of the initial degradation) of the baseline $\mathscr{Y}$ in 10 trials.

In this work, three variations of rendered force were explored. For each of these parameters, 10 adaptive trials were explored in both directions of variation, and each user underwent the experiment twice. Thus, a total of 120 experimental trials were conducted per user. The trials were pre-randomized to attenuate learning effects. Between trials, users were also re-acclimated to the baseline case $\mathscr{Y}$. The experimental workflow is depicted in Fig. 6.

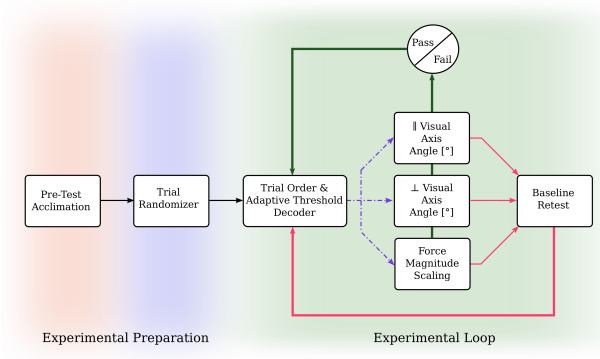

Fig. 6: The tests initiate with a pre-test whereby users prove proficiency in the ground truth baseline test. Trials are then randomized, and then experimental parameters are adjusted automatically via the adaptive threshold algorithm. Between test cases, users are required to retest the baseline case.

The user operated a 3DOF haptic device while viewing the palpation simulation on a standard computer monitor. The haptic device was positioned generally to the right of the simulation, consistent with the right-handedness of all four subjects. During trials, the operator was asked to refrain from seeking any auxiliary haptic cues, e.g. brushing the forearm on the edge of the desk or resting the elbow on a fixed surface. The typical trial workspace is illustrated in Fig. 7.

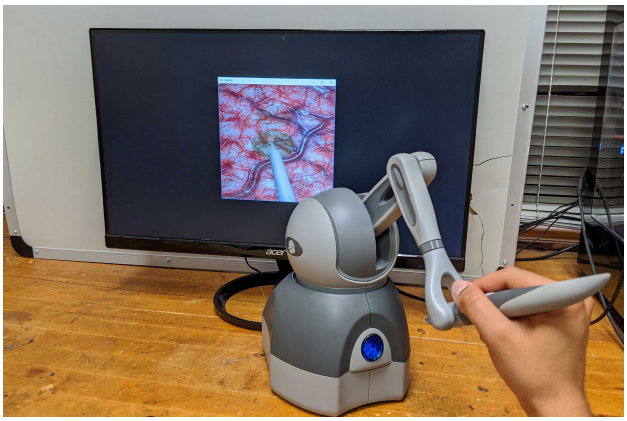

Fig. 7: The typical experimental setup. The user interacts with the simulation both visually and haptically through a stylus haptic device, through which motion commands are sent and force feedback is received.

III. Results

A. Force Orientation Parallel to Visual Axis

Parameter **A** targeted orientation error in force feedback coincident with the camera viewing angle. The ground truth force vector $\vec{F}$ was rotated about the axis both parallel to the horizontal image plane axis and orthogonal to the camera view axis. The positive (rotated toward viewer) and negative (rotated away from viewer) initiated at $\pm 40^\circ$. The adaptive thresholds results are shown in Fig. 8.

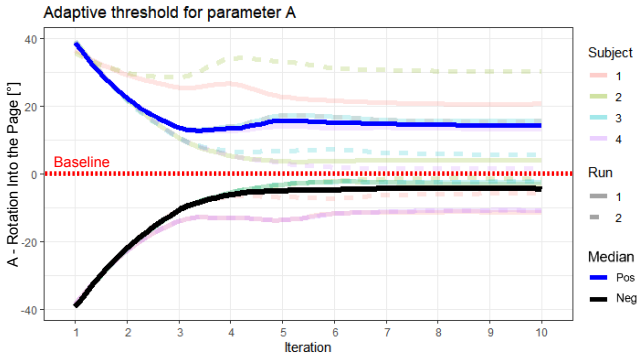

Fig. 8: Tolerance thresholds for orientation degradation towards and away from the user. 0° represents ground truth.

The final median positive and negative thresholds were 14.4° and - 4.4° respectively.

B. Force Orientation Orthogonal to Visual Axis

Parameter **B** targeted orientation error in force feedback observed as force rotated clockwise (CW) or counterclockwise (CCW). The ground truth force vector $\vec{F}$ was rotated about the camera visual axis. The positive (rotated CCW) and negative (rotated CW) error threshold initiated at $\pm 40^\circ$. The adaptive threshold results are presented in Fig. 9.

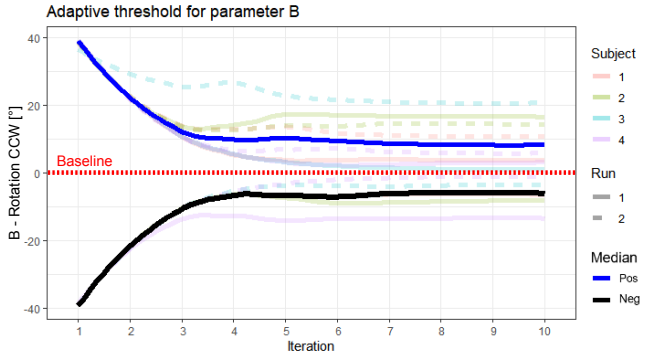

Fig. 9: Tolerance thresholds for orientation degradation observed as CCW and CW from the viewer. 0° represents ground truth.

The final median positive and negative thresholds were 8.21° and - 6.05° respectively.

C. Force Magnitude

The force parameter **C** scaled the force magnitude. The negative error threshold started initiated with half the true force magnitude, and the positive initiated with 150% force magnitude. The adaptive thresholds are shown in Fig. 10.

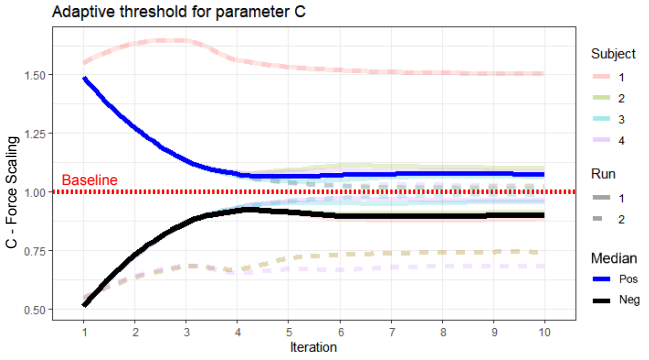

Fig. 10: Tolerance thresholds for force feedback magnitude scaling. The ground truth scale is 1.

The final median positive and negative thresholds were 1.08 and 0.899 respectively. Table I shows the median final threshold values for each parameter.

Threshold		Median
A	+	+14.4°
	-	-4.4°
B	+	+8.21°
	-	-6.05°
C	+	×1.08
	-	×0.899

TABLE I: Median Adaptive Thresholds

IV. Conclusion

This preliminary experiment introduced a cursory user study that aimed to determine the error tolerance in haptic feedback for surgeons to complete a simple palpation task on a simulated tissue patch. Each user was provided with precise visual feedback and degraded force cues either in the form of deviated orientation or magnitude. A total of eight experiments with four subjects were performed with adaptive thresholding methods to establish baseline positive and negative error tolerance thresholds in each of three parameters. These parameters are described in Fig. 5.

A. Summary

Overall, the results of this preliminary study suggest operator sensitivity is not necessarily symmetric to orientation error in vision-based force estimation. In particular, users tended to demonstrate an *increased robustness in force orientation error away and to the left* (CCW). This is observed in the greater threshold magnitudes for positive directions in parameters **A** and **B**. One possible explanation arises when considering typical grasps for right-handed users in stylus haptic interaction (such as during handwriting). A fulcrum is formed with the hand while the load generates forces at the stylus tip away and to the left. When the ground truth force is rotated towards the direction of the lever link (toward the user and to the right), less force is perceived at the fulcrum, resulting in degraded perception.

In this study, users maintained acceptable palpation performance even if force magnitude was scaled by about 10%. For the positive threshold of force magnitude, 150% of the pop-through force (2.3 N) saturates the haptic device output at 3.3N. This might result in undesired cues for artificially improving performance as observed in two outlier runs. In these two runs the subject did not succeed again after the initial trial. In contrast, no subject successfully completed the palpation task with attenuated force magnitude on the first trial. This suggests that a lack of haptic cues is considerably detrimental to task performance. Since the displayed force orientation was in the z-axis and not altered in parameter **C**, handedness is not suspected to affect these results.

In general, the results of this study suggest that when considering accuracy of non-contact vision-based force estimation for palpation error tolerance in :

i) orientation is greater away from the user;
ii) orientation is greater in the direction away from the user's dominant hand;
iii) force magnitude is generally symmetric.

Force estimation confidence should thus consider user handedness and viewing perspective.

B. Future Work

This work focused on the surgical task - palpation, a well established diagnostic surgical practice. Moving forward, the authors are interested in exploring five main directions: (1) incorporate more extensive psychophysical experimental methodologies and measures; (2) apart from examining tissue indentation depth during the palpation task, experimentally compare the force error tolerance results from other common surgical performance evaluation metrics; (3) design a realistic noisy force feedback model rather than a static offset in only orientation or magnitude; (4) allowing users to adjust visual feedback viewpoint as they prefer; and finally (5) replication with a real telerobotic system and physical tissue phantoms. The results in this work serve as a baseline and proof of concept implementation for these future directions.

ACKNOWLEDGEMENTS

The authors would like to thank Hassan Rashid, Isabella Yung, and the other members of the Perceptual-robotics and Automation (PandA) laboratory from Trinity College in Hartford, CT for technical assistance and support.

REFERENCES

[1] N. Enayati, E. De Momi, and G. Ferrigno, "Haptics in robot-assisted surgery: Challenges and benefits," *IEEE reviews in biomedical engineering*, vol. 9, pp. 49–65, 2016.

[2] O. A. Van der Meijden and M. P. Schijven, "The value of haptic feedback in conventional and robot-assisted minimal invasive surgery and virtual reality training: a current review," *Surgical endoscopy*, vol. 23, no. 6, pp. 1180–1190, 2009.

[3] Y.-H. Su, I. Huang, K. Huang, and B. Hannaford, "Comparison of 3d surgical tool segmentation procedures with robot kinematics prior," in *2018 IEEE/RSJ International Conference on Intelligent Robots and Systems (IROS)*. IEEE, 2018, pp. 4411–4418.

[4] Y.-H. Su, K. Huang, and B. Hannaford, "Real-time vision-based surgical tool segmentation with robot kinematics prior," in *Medical Robotics (ISMR), 2018 International Symposium on*. IEEE, 2018, pp. 1–6.

[5] L. A. Jones and H. Z. Tan, "Application of psychophysical techniques to haptic research," *IEEE transactions on haptics*, vol. 6, no. 3, pp. 268–284, 2012.

[6] S. M. N. Melder and A. B. W. H. J. Wann, "Psychophysical size discrimination using multi-fingered haptic interfaces," *Perception*, pp. 274–281, 2004.

[7] B. Hannaford, J. Dosher, and S. Venkatachalam, "Haptic exploration of spheres: Techniques and initial experiments," in *2010 IEEE Haptics Symposium*. IEEE, 2010, pp. 9–15.

[8] C. Gaudeni, L. Meli, L. A. Jones, and D. Prattichizzo, "Presenting surface features using a haptic ring: A psychophysical study on relocating vibrotactile feedback," *IEEE transactions on haptics*, vol. 12, no. 4, pp. 428–437, 2019.

[9] M. Di Luca and A. Mahnan, "Perceptual limits of visual-haptic simultaneity in virtual reality interactions," in *2019 IEEE World Haptics Conference (WHC)*. IEEE, 2019, pp. 67–72.

[10] I. Jiang and B. Hannaford, "Comparison of reaction times while walking," in *2015 IEEE International Conference on Rehabilitation Robotics (ICORR)*. IEEE, 2015, pp. 345–349.

[11] T. Heo, K. Huang, and H. J. Chizeck, "Performance evaluation of haptically enabled semg," in *2018 International Symposium on Medical Robotics (ISMR)*. IEEE, 2018, pp. 1–6.

[12] J. Yan, K. Huang, T. Bonaci, and H. J. Chizeck, "Haptic passwords," in *2015 IEEE/RSJ International Conference on Intelligent Robots and Systems (IROS)*. IEEE, 2015, pp. 1194–1199.

[13] J. J. Abbott, P. Marayong, and A. M. Okamura, "Haptic virtual fixtures for robot-assisted manipulation," in *Robotics research*. Springer, 2007, pp. 49–64.

[14] K. Huang, P. Lancaster, J. R. Smith, and H. J. Chizeck, "Visionless tele-exploration of 3d moving objects," in *2018 IEEE International Conference on Robotics and Biomimetics (ROBIO)*. IEEE, 2018, pp. 2238–2244.

[15] K. Huang, D. Chitrakar, F. Rydén, and H. J. Chizeck, "Evaluation of haptic guidance virtual fixtures and 3d visualization methods in telemanipulation—a user study," *Intelligent Service Robotics*, pp. 1–13, 2019.

[16] K. Huang, Y.-H. Su, M. Khalil, D. Melesse, and R. Mitra, "Sampling of 3dof robot manipulator joint-limits for haptic feedback," in *2019 IEEE 4th International Conference on Advanced Robotics and Mechatronics (ICARM)*. IEEE, 2019, pp. 690–696.

[17] E. P. Westebring-van der Putten, R. H. Goossens, J. J. Jakimowicz, and J. Dankelman, "Haptics in minimally invasive surgery–a review," *Minimally Invasive Therapy & Allied Technologies*, vol. 17, no. 1, pp. 3–16, 2008.

[18] W. Khaled, S. Reichling, O. Bruhns, H. Boese, M. Baumann, G. Monkman, S. Egersdoerfer, D. Klein, A. Tunayar, H. Freimuth *et al.*, "Palpation imaging using a haptic system for virtual reality applications in medicine," in *Perspective In Image-Guided Surgery*. World Scientific, 2004, pp. 407–414.

[19] K. Veluvolu and W. Ang, "Estimation and filtering of physiological tremor for real-time compensation in surgical robotics applications," *The International Journal of Medical Robotics and Computer Assisted Surgery*, vol. 6, no. 3, pp. 334–342, 2010.

[20] B. W. O'Malley Jr, G. S. Weinstein, and N. G. Hockstein, "Transoral robotic surgery (tors): glottic microsurgery in a canine model," *Journal of Voice*, vol. 20, no. 2, pp. 263–268, 2006.

[21] S. M. Prasad, S. M. Prasad, H. S. Maniar, C. Chu, R. B. Schuessler, and R. J. Damiano Jr, "Surgical robotics: impact of motion scaling on task performance," *Journal of the American College of Surgeons*, vol. 199, no. 6, pp. 863–868, 2004.

[22] M. Matinfar, C. Baird, A. Batouli, R. Clatterbuck, and P. Kazanzides, "Robot-assisted skull base surgery," in *2007 IEEE/RSJ International Conference on Intelligent Robots and Systems*. IEEE, 2007, pp. 865–870.

[23] M. Hoeckelmann, I. J. Rudas, P. Fiorini, F. Kirchner, and T. Haidegger, "Current capabilities and development potential in surgical robotics," *International Journal of Advanced Robotic Systems*, vol. 12, no. 5, p. 61, 2015.

[24] K. Moorthy, Y. Munz, A. Dosis, J. Hernandez, S. Martin, F. Bello, T. Rockall, and A. Darzi, "Dexterity enhancement with robotic surgery," *Surgical Endoscopy and Other Interventional Techniques*, vol. 18, no. 5, pp. 790–795, 2004.

[25] B. T. Bethea, A. M. Okamura, M. Kitagawa, T. P. Fitton, S. M. Cattaneo, V. L. Gott, W. A. Baumgartner, and D. D. Yuh, "Application of haptic feedback to robotic surgery," *Journal of Laparoendoscopic & Advanced Surgical Techniques*, vol. 14, no. 3, pp. 191–195, 2004.

[26] P. S. Angelica I. Aviles, Arturo Marban, "A recurrent neural network approach for 3d vision-based force estimation," *Image Processing Theory, Tools and Applications (IPTA), 2014 4th International Conference*, 2014.

[27] C. Gao, X. Liu, M. Peven, M. Unberath, and A. Reiter, "Learning to see forces: Surgical force prediction with rgb-point cloud temporal convolutional networks," in *OR 2.0 Context-Aware Operating Theaters, Computer Assisted Robotic Endoscopy, Clinical Image-Based Procedures, and Skin Image Analysis*. Springer, 2018, pp. 118–127.

[28] L. Cheng, "Computation and measurement of force and tissue damage for the grasper-tissue interface in robot-assisted minimal invasive surgery," *Doctoral thesis, University of Washington*.

[29] Y.-H. Su, K. Huang, and B. Hannaford, "Multicamera 3d reconstruction of dynamic surgical cavities: Camera grouping and pair sequencing," in *2019 International Symposium on Medical Robotics (ISMR)*. IEEE, 2019, pp. 1–7.

[30] ——, "Multicamera 3d reconstruction of dynamic surgical cavities: Autonomous optimal camera viewpoint adjustment," in *Medical Robotics (ISMR), 2020 International Symposium on*. IEEE, 2020.

[31] H. Delingette and N. Ayache, "Soft tissue modeling for surgery simulation," *Handbook of Numerical Analysis*, vol. 12, pp. 453–550, 2004.

[32] U. Meier, O. López, C. Monserrat, M. C. Juan, and M. Alcaniz, "Real-time deformable models for surgery simulation: a survey," *Computer methods and programs in biomedicine*, vol. 77, no. 3, pp. 183–197, 2005.

[33] G. Picinbono, H. Delingette, and N. Ayache, "Nonlinear and anisotropic elastic soft tissue models for medical simulation," in *Proceedings 2001 ICRA. IEEE International Conference on Robotics and Automation (Cat. No. 01CH37164)*, vol. 2. IEEE, 2001, pp. 1370–1375.

[34] S. Kumar, G. Liu, D. W. Schloerb, and M. A. Srinivasan, "Viscoelastic characterization of the primate finger pad in vivo by microstep indentation and three-dimensional finite element models for tactile sensation studies," *Journal of biomechanical engineering*, vol. 137, no. 6, 2015.

[35] F. B. De Casson and C. Laugier, "Modeling the dynamics of a human liver for a minimally invasive surgery simulator," in *International Conference on Medical Image Computing and Computer-Assisted Intervention*. Springer, 1999, pp. 1156–1165.

[36] K. Lindgren, K. Huang, and B. Hannaford, "Towards real-time surface tracking and motion compensation integration for robotic surgery," in *2017 IEEE/SICE International Symposium on System Integration (SII)*. IEEE, 2017, pp. 450–456.